Development of a High-Energy-Density Lithiated Silicon-Sulfur Full Cell with Enhanced Stability and Longevity

Guiping Li, Barbora Balcarova, Thorsten Schultz, Changjiang Bai, Moritz Exner, Hui Wang, Yanchen Liu, Nicola Pinna, Norbert Koch, Philipp Adelhelm, and Michael J. Bojdys**

Guiping Li, Prof. Michael Janus Bojdys
Department of Chemistry & Center for the Science of Materials Berlin (CSMB), Humboldt-Universität zu Berlin, Brook-Taylor-Str. 2, 12489, Germany

Barbora Balcarova , Changjiang Bai, Moritz Exner, Hui Wang, Yanchen Liu
Department of Chemistry & IRIS Adlershof, Humboldt-Universität zu Berlin, Brook-Taylor-Str. 2, 12489, Germany

Dr. Thorsten Schultz, Prof. Norbert Koch
Humboldt-Universität zu Berlin, Institut für Physik, Institut für Chemie, IRIS Adlershof, Zum Großen Windkanal 2, 12489 Berlin, Germany,
Helmholtz-Zentrum Berlin, Hahn-Meitner-Platz 1, 14109 Berlin, Germany

Prof. Philipp Adelhelm
Department of Chemistry & Center for the Science of Materials Berlin (CSMB), Humboldt-Universität zu Berlin, Brook-Taylor-Str. 2, 12489, Germany
Helmholtz-Zentrum Berlin, Hahn-Meitner-Platz 1, 14109 Berlin, Germany

*E-mail: liguipin@hu-berlin.de; m.j.bojdys.02@cantab.net

Keywords: *lithium-sulfur batteries, electrochemical stability, energy storage materials*

Abstract

Silicon-sulfur (Si-S) batteries represent a promising energy storage solution due to their high theoretical energy density. However, practical applications have been hindered by substantial volume expansion of silicon and the dissolution of sulfur species. Here, we combine a triazine-based graphdiyne-coated silicon (TzG@Si) anode and a sulfurized polyacrylonitrile (S@PAN) cathode into a cell that uniquely mitigates the volume expansion of silicon and prevents sulfur migration. Notably, the integration of TzG@Si and S@PAN results in the formation of a stable, LiF-rich solid-electrolyte interphase (SEI) on both electrodes, significantly enhancing the cycling stability. The optimized cell exhibits an energy density of 414.3 Wh kg^{-1} based on electrodes' mass (Si anode and S@PAN cathode), with a capacity retention exceeding 80% after 400 cycles. Moreover, we explore the lithiation mechanisms within the S@PAN cathode, revealing that controlled voltage windows can further improve performance by preventing deep discharge. Our findings suggest that by engineering the electrodes, this Si-S battery system can achieve long cycle life and high energy density. This work not only advances the understanding of Si-S battery chemistry but also highlights the importance of synergistic electrode and electrolyte design in developing practical solutions for high-energy-density batteries.

Introduction

The urgent global shift towards sustainable energy systems necessitates advancements in energy storage technologies, particularly in the face of dwindling non-renewable fossil fuel resources and escalating energy demands.[1] Lithium-ion batteries (LIBs), which currently dominate the commercial battery market, are approaching their theoretical limits in energy density, typically ranging from 100 to 265 Wh kg^{-1}.[2] This limitation has spurred research into alternative high-energy-density systems, notably lithium-sulfur (Li-S) batteries, recognized for their potential ultra-high theoretical energy density of 2500 Wh kg^{-1} and environmental advantages.[3] However, Li-S technologies face significant challenges, such as the "shuttle effect" due to polysulfide dissolution and dendrite growth on lithium metal anodes, which hinder their practical application.[4] On the anode front, silicon-based materials are considered a prime candidate for high-energy-density batteries due to their impressive capacity of 3579 mA h g^{-1}, second only to lithium metal. Their abundance and environmental friendliness further augment their suitability as an alternative in battery technologies.[5]

However, these materials are challenged by substantial volume expansions during charge/discharge cycles, exceeding 300% particularly when high ratios of silicon are used in the electrodes. This expansion can cause the silicon particles to fracture under mechanical stress, leading to a loss of contact with the current collector and a subsequent decrease in battery capacity. Various strategies have been deployed to enhance performance, such as refining the nanostructures,[6] embedding the silicon particles within a carbon matrix,[7] developing specifically tailored binders,[8] and enhancing the electrolytes.[9] In contrast, a sulfurized polyacrylonitrile (S@PAN) was exploited by Wang at 2002,[10] which employs a solid–solid conversion mechanism that effectively addresses the dissolution of polysulfides, commonly associated with the shuttle effect. Although this material has a voltage loss (average discharge voltage at ~1.8 V) compared to the traditional sulfur cathode (average discharge voltage at ~2.2 V), it still potentially afford a high energy density. The compatibility of carbonate electrolyte makes S@PAN a good applicant to match graphite or silicon anodes.

Addressing these limitations, our research focuses on the development of a novel full cell system (**Figure 1a**) utilizing silicon coated by triazine-based graphdiyne (TzG) at the anode and S@PAN at the cathode to overcome the traditional barriers associated with Li-S batteries. The TzG@Si anode benefits from the incorporation of silicon particles into a π-conjugated

polymer network, enhancing electrical connectivity and accommodating volume changes during cycling, thus mitigating the common issue of capacity fading seen in high silicon-content electrodes.

Our innovative TzG@Si/S@PAN full cell system, first of its kind, demonstrated an areal capacity exceeding 2.0 mAh cm^{-2} and an energy density of 414.3 Wh kg^{-1} in a coin cell configuration. This study not only showcases a strategic overcoming of the well-documented limitations of high-energy-density batteries but also introduces a novel material synthesis approach promising for future battery technology. This work lays the groundwork for further development of stable, high-energy-density battery systems, crucial for advancing beyond traditional NMC-based energy storage systems.

Results and discussion

Design and structures of the TzG@Si and S@PAN electrodes

The TzG@Si anode consists of silicon nanoparticles encapsulated within a porous, semiconducting polymer matrix of triazine-based graphdiyne (TzG). Growth of the polymer matrix around the silicon particles is initiated and templated directly by the copper current collector. Previous work has shown that the TzG polymer acts as a robust binder and facilitates charge transport, which enhances the electrode performance.[11] By adjusting the TzG to silicon weight ratio to 25/75, a uniform electrode structure was formed, displaying silicon particles uniformly distributed and embedded in 2D polymer sheets (SEM, **Figure 1b** and EDX, **Figure S1**). Stability and integrity of the TzG polymer network were confirmed by Fourier-transform infrared spectra (FTIR) and Raman spectroscopy. The FTIR spectrum (**Figure 1c**) indicated a reduction in the ≡C-H (3200 to 3300 cm^{-1}) stretching vibrations in the alkynyl groups post-polymerization.[12] The Raman spectrum (**Figure 1d**) revealed characteristic bands, including diyne C≡C at 2209 cm^{-1}, triazine C=N at 1411 cm^{-1}, phenyl C=C at 1604 cm^{-1}, and crystalline Si-Si bonds at 518 cm^{-1}.[13]

The sulfurized polyacrylonitrile (S@PAN) cathode was synthesized by combining elemental sulfur powder (S_8) with conventional polyacrylonitrile (PAN). This process leads to the formation of a polymer where S_8 is opened and integrated as smaller sulfur molecules (S_x, x = 1…4) within the polymer network. The resulting S@PAN was presented as a bulk powder (**Figure 1e**), and EDX analysis (**Figure S2**) demonstrated an even distribution of C, N, and S atoms. Elemental analysis (**Table S1**) showed that the sulfur content in S@PAN was

approximately 40 wt%. Successful synthesis was confirmed through FTIR, Raman, and solid-state NMR (ssNMR) spectroscopy. FTIR analysis (**Figure 1f**) highlighted the disappearance of the C≡N (2247 cm−1) and C-H (2930 cm^{-1}) bands, and the emergence of new S-S (513 cm^{-1}), C-S (657 cm^{-1}), N-S (936 cm^{-1}), and C=N-C=C (1493 cm^{-1}, 1535 cm^{-1}) bonds.[14] Raman spectroscopy (Figure 1f) further clarified the sulfur chemical bonding and identified two distinct peaks corresponding to the partial carbonization of the S@PAN polymer network, the D band at 1326 cm^{-1} and the G band at 1552 cm^{-1}.[14-15] The ^{13}C CP-MAS NMR spectrum of S@PAN (**Figure S3**) differed from PAN, with signals at 150 ppm and 125 ppm attributed to the sp^2 hybridized conjugated carbon of C=N and C=C, respectively, indicating a slight shielding effect.[16] X-ray diffraction (XRD) (**Figure S4**) revealed that S@PAN is amorphous, with a broad peak corresponding to the carbon backbone of the polymer.

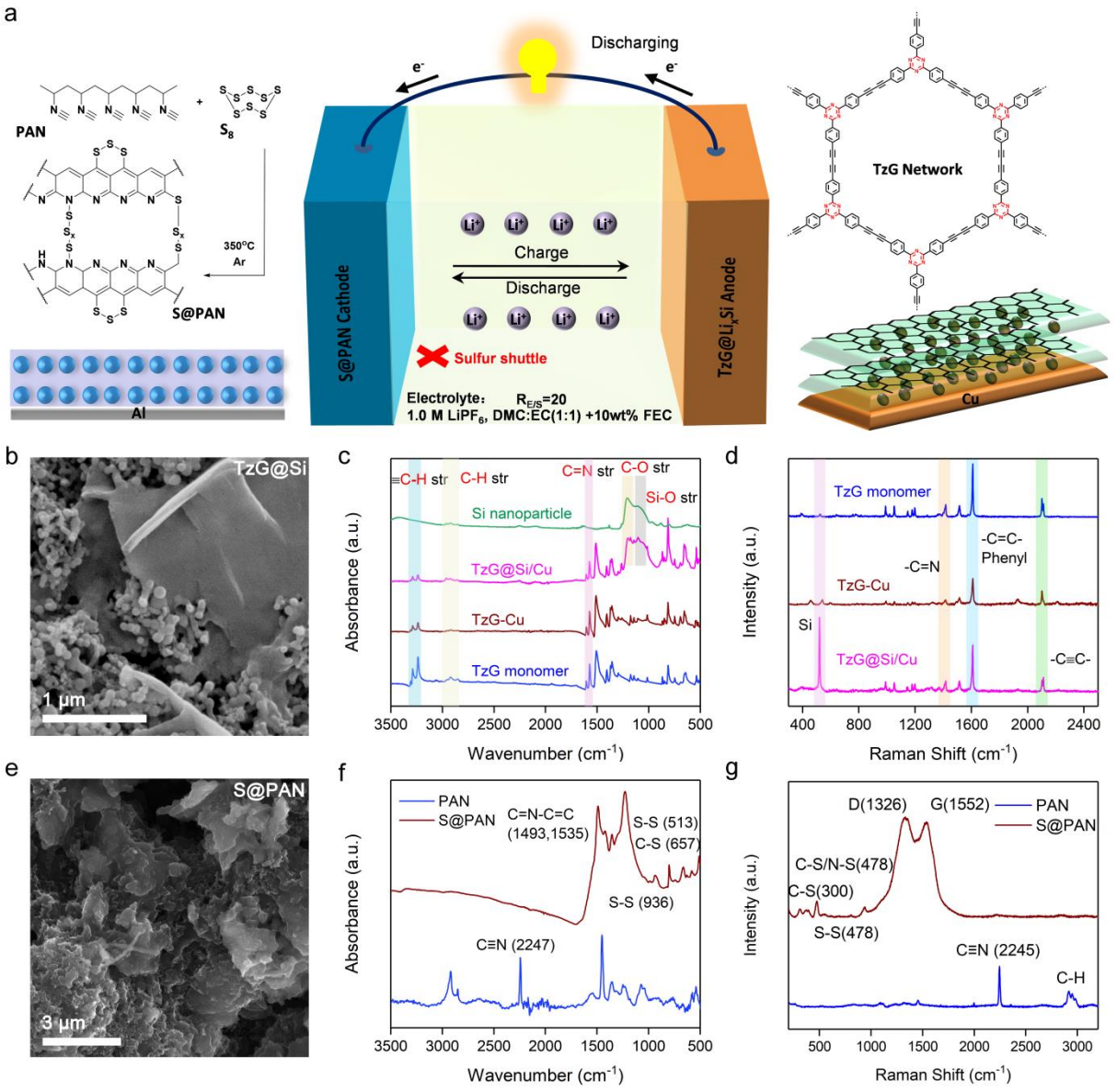

Figure 1. (**a**) Schematic representation of the S@PAN‖TzG@Li_xSi full cell; (**b**, **c**, and **d**) SEM, FTIR, and Raman spectra of the TzG@Si anode, respectively; (**e**, **f**, and **g**) SEM, FTIR, and Raman spectra of the S@PAN cathode, respectively.

Electrochemical characterizations of TzG@Si-Li and S@PAN-Li half cells

The electrochemical performance of the TzG@Si anode and S@PAN cathode was evaluated in half-cell configurations against lithium metal. Both TzG@Si-Li and S@PAN-Li half cells used the same electrolyte (1.0 M $LiPF_6$, DMC:EC(1:1) +10wt% FEC) to ensure consistency in testing conditions. Initially, cyclic voltammetry (**Figure 2a**) was conducted to analyze the charge/discharge mechanisms of the TzG@Si electrode. The initial response current was low, since during the initial lithiation of crystalline silicon might involve sluggish kinetics and limited ion diffusion. While, after two scanning rounds, the electrode's activity notably improved. A distinct lithiation peak at 0.13 V (Peak 1) indicates the lithiation of silicon to form amorphous $Li_{15}Si_4$, while the subsequent delithiation peaks (Peak 2 for partial and Peak 3 for complete removal) reflect the extraction of Li^+ ions from $Li_{15}Si_4$.[17] During the first lithiation cycle, the TzG@Si anode demonstrated a high initial lithiation/delithiation capacity of 4356/3011 mAh g^{-1} with a coulombic efficiency (CE) of approximately 70%. From the second cycle onward, CE increased to above 98%, reaching as high as 99.5% in later cycles, suggesting that the majority of the SEI forms in the initial cycle. The silicon anode also showed excellent rate performance (**Figure S5**), maintaining a high capacity of 2046.6 mAh g^{-1} at 1 C rate. With a specific lithiation capacity of 2378.1 mAh g^{-1} taken in the third cycle as a reference, TzG@Si retained 84.9% capacity after 100 cycles (2019.1 mAh g^{-1}), indicating stable performance.

In contrast, the first cycle of cyclic voltammetry for the S@PAN cathode (**Figure 2d**) revealed significant differences, characterized by a large and robust peak between 1.5-1.0 V and a broad peak from 1.0-0.5 V, suggesting complex lithiation processes involving various sites and species.[18] In subsequent cycles, cathodic peaks shifted to higher voltages and stabilized, indicating a typical activation was underwent during first cycle, with improved conductivity and/or a change in the reaction mechanism. Initially, the S@PAN cathode also faced a low CE of around 70%, attributed primarily to the formation of a cathode electrolyte interphase (CEI) and some irreversible capacity due to the carbonized polymer backbone. From the second cycle, CE significantly improved, reaching 98.0% and even up to 99.8% in later cycles. The S@PAN cathode also displayed strong rate performance (**Figure S6**),

achieving a high capacity of 961.9 mAh g^{-1} at 1 C. Using the specific lithiation capacity of 1122.3 mAh g^{-1} from the third cycle (with the first two cycles serving as activation), the S@PAN cathode maintained 91.9% capacity after 200 cycles (1030.2 mAh g^{-1}), demonstrating exceptional stability.

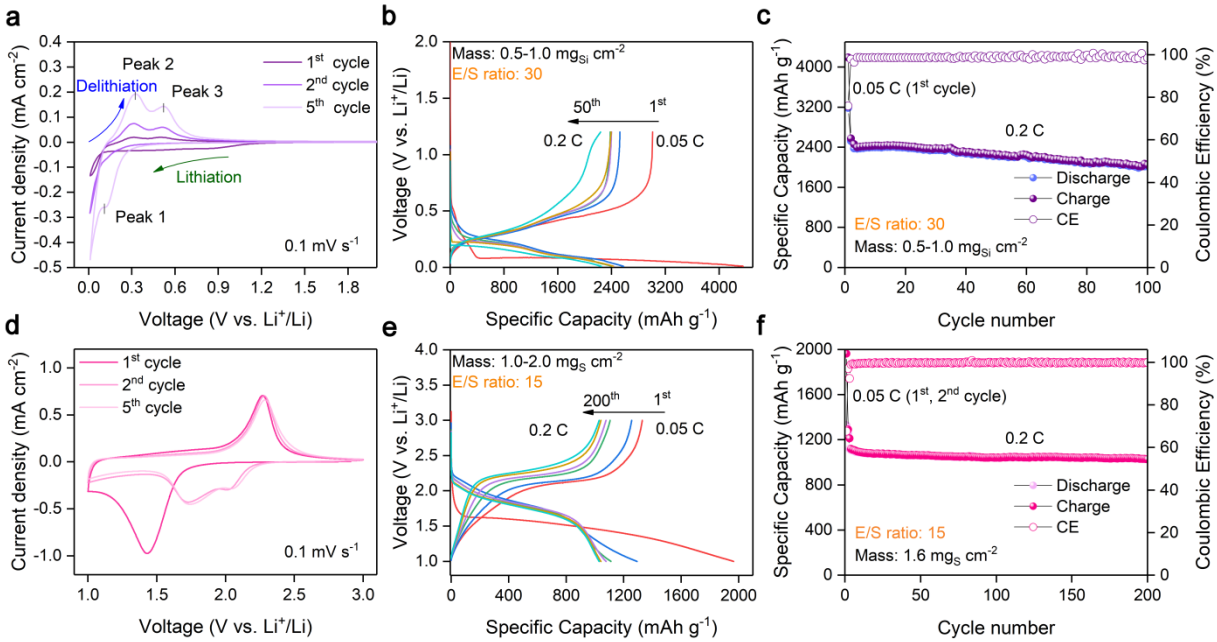

Figure 2. (**a**) Cyclic voltammetry of the TzG@Si-Li half-cell (scanning rate: 0.1 mV s^{-1}); (**b**) Discharge-charge profiles of the TzG@Si-Li half-cell at 0.2 C (initial two cycles at 0.05 C, voltage range 0.01-1.2 V vs. Li^+/Li); (**c**) Cycling stability of TzG@Si at 0.2 C (initial one cycles at 0.05 C); (**d**) Cyclic voltammetry of the S@PAN-Li half-cell (scanning rate: 0.1 mV s^{-1}); (**e**) Discharge-charge profiles of the S@PAN-Li half-cell at 0.2 C (initial two cycles at 0.05 C, voltage window 1.0-3.0 V vs. Li^+/Li); (**f**) Cycling stability of S@PAN at 0.2 C (initial two cycles at 0.05 C).

Electrochemical performance of the lithiated TzG@Si/ S@PAN full cell

Prior to the assembly of the full cell, a pre-lithiation step was conducted on the TzG@Si anode to introduce lithium source.[19] The cell was configured with a low negative-to-positive capacity ratio of 1.5:1 (nominal capacity: 2.0 mAh with anode, 1.34 mAh with cathode), and a fresh S@PAN electrode was utilized on the cathode side. Charge–discharge curves depicted in **Figure 3a** demonstrate the specific capacities achieved by the TzG@Si and S@PAN electrodes, respectively, reaching 2576.0 mAh g^{-1} and 1293.2 mAh g^{-1} at a 0.2 C rate. It was posited that the selected voltage window critically impacts both the capacity and stability of the full cell. The electrochemical behaviors under different cutoff voltages of 0.8 V and 1.0 V were subsequently evaluated. **Figure 3b** illustrates the cyclic voltammetry of the TzG@Si/S@PAN full cell, which closely mimics the CV profile of the S@PAN-Li half-cell

with cathodic peaks shifting to lower voltages, reflecting the potential influence of the silicon component (considered 0 V relative to lithium).

The rate capability and cyclic performance of the TzG@LixSi/S@PAN full cells are presented in **Figures 3c**, **3d**, and **3e**. At a cutoff voltage of 0.8 V, the full cell delivered initial capacities of 915 mAh g^{-1} and 690.8 mAh g^{-1} after 100 cycles based on sulfur mass. The estimated energy densities were 414.3 Wh kg^{-1} (average discharge voltage of 1.34 V) at a cutoff voltage of 0.8 V and 372.9 Wh kg^{-1} (average discharge voltage of 1.39 V) at a cutoff voltage of 1.0 V. (Calculation details were presented in SI). Regarding rate capabilities, the full cell demonstrated a capacity of 955.3 mAh g^{-1} at 0.1 C and achieved 619.1 mAh g^{-1} at 1 C for the 0.8 V cutoff, whereas at 1.0 V, the capacity was 795.3 mAh g^{-1} at 0.1 C, reducing to 447.1 mAh g^{-1} at 1 C. Long-term cycling performance, shown in **Figure 3e**, revealed a capacity retention of 79.6% over 400 cycles at a 1.0 V cutoff, but only 65.1% at 0.8 V, indicating that deeper discharge levels yield higher energy but lower stability.

The in-situ electrochemical impedance spectroscopy (EIS) analysis of the TzG@Li_xSi/S@PAN full cell is documented in **Figure S7a-f**. The pristine full cell displayed a modest semicircle in the high-frequency range, which is indicative of the resistance (R_{SEI}) associated with the SEI layer from Li_xSi (**Figure S7b**).[20] As lithiation progressed (**Figure S7c**), a new semicircle at mid-frequency appeared, representing the charge-transfer resistance (R_{ct}). This resistance decreased with further lithiation, indicating improved conductivity within the electrode. In contrast, during delithiation (charging), the R_{ct} semicircle expanded, reflecting a reduction in conductivity of the electrode materials as they underwent reversible conversion.[21] Importantly, the SEI layer's semicircle remained largely unchanged throughout the cycling process, suggesting the establishment of a stable SEI layer with low resistance that aids in the diffusion of lithium ions.

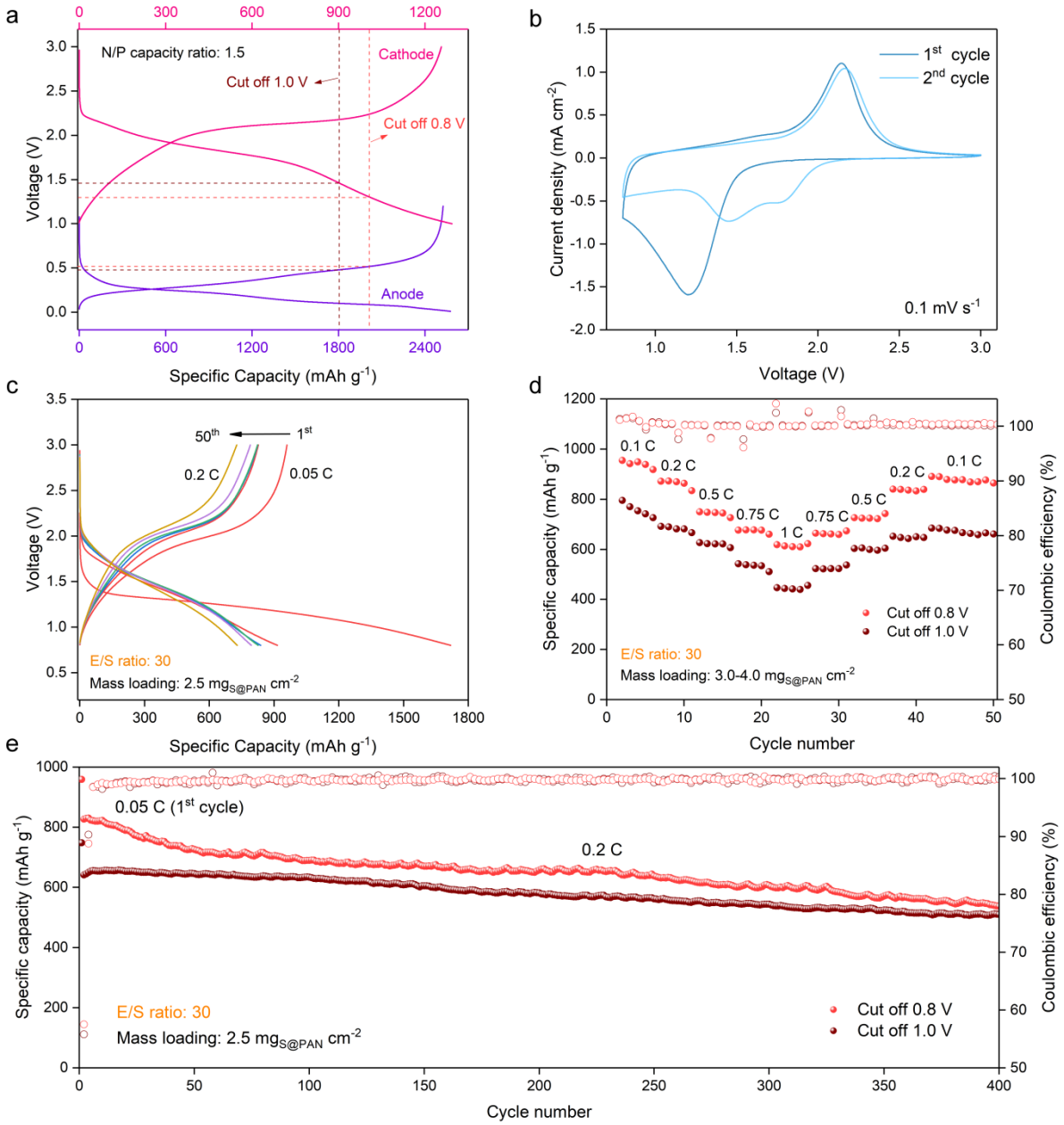

Figure 3. (**a**) Charge/discharge curves for S@PAN vs. Li^+/Li and TzG@Si vs. Li^+/Li in half cells; (**b**) Cyclic voltammetry of the lithiated TzG@Si/S@PAN full cell (scanning rate: 0.1 mV s^{-1}); (**c**) Discharge-charge profiles of the TzG@Si/S@PAN full cell at 0.2 C (initial two cycles at 0.05 C, voltage range 0.8-3.0 V; (**d**) Rate performance of the lithiated TzG@Si/S@PAN full cell across various current densities; (**e**) Long-term cycling performance of the lithiated TzG@Si/S@PAN full cell at 0.2 C.

Evolution of the composition and morphology of the electrodes for TzG@Li_xSi/S@PAN full cell

The full cell's stability significantly depends on its ability to handle the challenges of volume expansion and pulverization during the alloying reaction.[22] To elucidate these changes, we

characterized the electrodes at various stages: the pristine condition (I), after the first delithiation (II), and following 400 delithiation cycles using scanning electron microscopy (SEM) as depicted in **Figure 4a-d**. Initially, the TzG@Li_xSi electrodes show a uniform surface with spherical silicon particles averaging 500 nm, formed post full pre-lithiation (**Figures 4a(I)** and **b(I)**), as opposed to the un-prelithiated TzG@Si anode (**Figure S8**). These spheres featured a homogenous, rich fluoride SEI layer confirmed by EDX analysis (**Figure S9**) and were enveloped by polymer sheets ensuring a crack-free surface.

Post a complete discharge-charge cycle, the lithiated silicon anode maintained its integrity without any structural changes compared to its original state (**Figures 4a(II**) and **b(II)**), and the spherical particles did not pulverize, showcasing the protective role of the TzG polymer networks. However, after 400 cycles, subtle cracks due to electrode expansion became visible at lower magnifications (**Figures 4a(III)** and **b(III)**), which might have also arisen during the SEM sample preparation process. The S@PAN cathodes displayed minimal morphological changes after the initial cycle (**Figures 4c** and **4d**) but started to form rounded aggregated particles after extensive cycling, suggesting growth and aggregation of CEI species, yet retaining excellent structural integrity even after 400 cycles.

X-ray photoelectron spectroscopy (XPS) was utilized to analyze the SEI and CEI components (**Figures 4e-h**). The XPS spectra of F1s and C1s (**Figures 4e** and **4f**) for the TzG@Si anodes before cycling display typical TzG polymer bonds (**Figure S10**), whereas post-cycling spectra illustrate a complex SEI consisting of organic $ROCO_2Li$ at 286.99 eV, inorganic Li_2CO_3 at 288.8 eV, and significant amounts of LiF at 685.8 eV.[22] The appearance of C-F bonds above 290.0 eV in the C1s spectra (**Figure 4e**) indicates the decomposition of fluoroethylene carbonate (FEC) component in the electrolyte.[23] The peak in the C1s spectrum at 282.5 eV (**Figure 4e**) was attributable to contamination from the XPS sample holder, not from the anode material itself. Generally, the C1s and F1s spectra of the silicon anode in our full cell system showed remarkable consistency across different stages, demonstrating that the robust SEI formed effectively mitigated the decomposition of other organic solvents, thus ensuring excellent capacity retention and high Coulombic efficiency. In the case of the S@PAN cathode, discussions centered around the XPS spectra of S2p and F1s (**Figure 4h** and **Figure 4g**). The S2p spectrum shown in **Figure 4g(I)** reveals the sulfur characteristics of a pristine S@PAN cathode, displaying bonds such as C-S (~162 eV), S-S_x (~164 eV), and weaker signals for S-N and S=N (~168 eV).[24] Post-lithiation, the S2p spectrum of the S@PAN electrode (**Figure S11**) showed that Li-S-S_x were the predominant species within the voltage

range of 0.8-3.0 V. The intensity of the S2p spectra diminished following lithiation and delithiation, indicative of CEI species coverage. As for the F1s spectra of S@PAN (**Figure 4h**), alongside the C-F bond signal at 688.3 eV from the PVDF binder and the –HCF from FEC component decomposition, a distinct LiF signal was also present at 686.5 eV. The compatibility of the carbonate electrolyte with FEC on both electrode sides led to the formation of robust solid electrode interphases, significantly bolstering the overall stability of the full cell system.

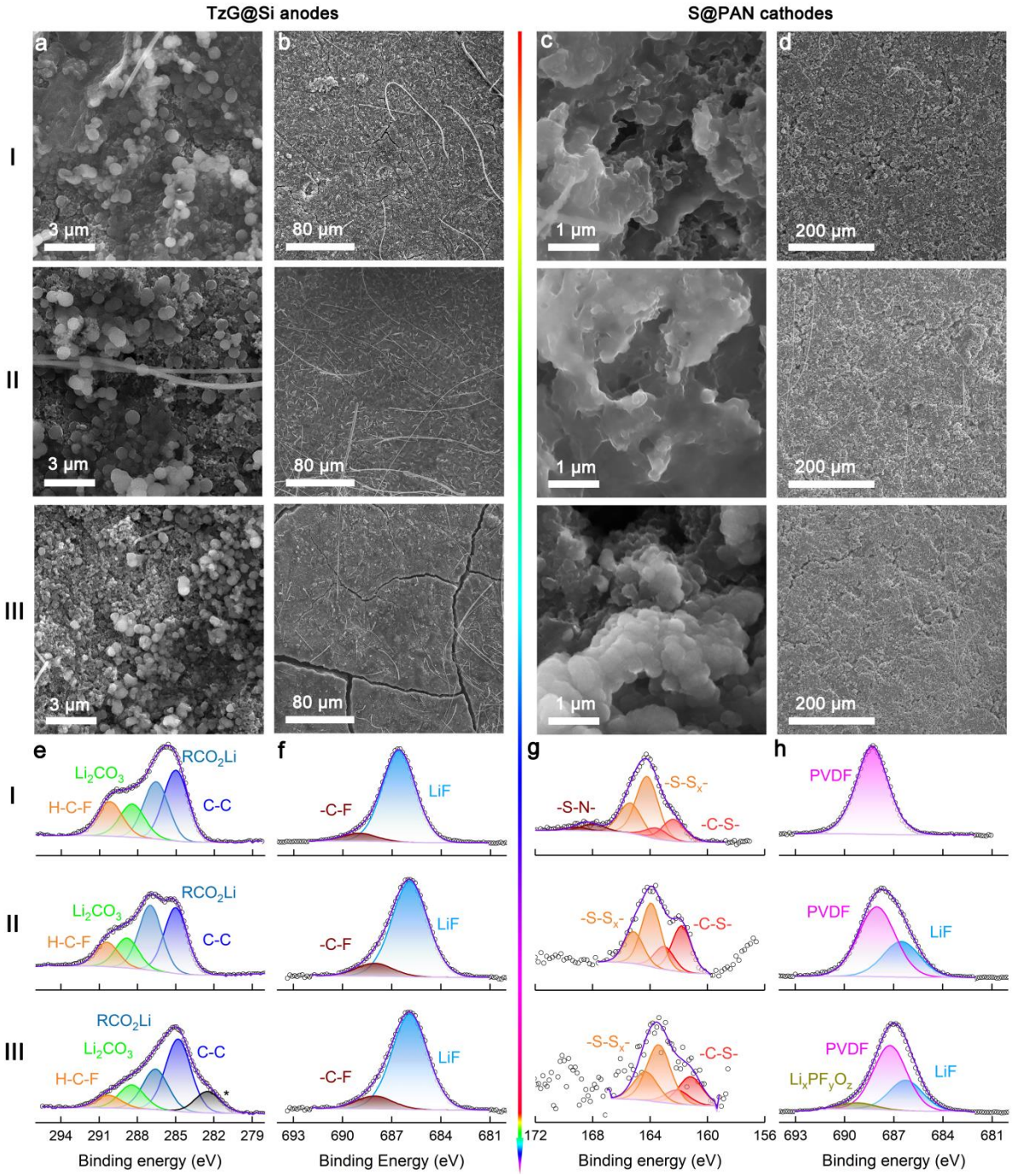

Figure 4. Characterization of TzG@Si electrodes in the full cell: (**a**, **b**) Scanning electron microscopy (SEM) images at different magnifications; (**e**, **f**) X-ray photoelectron spectroscopy (XPS) analyses of C1s and F1s spectra, respectively. Characterization of S@PAN electrodes in the full cell: (**c**, **d**) Scanning electron microscopy (SEM) images at different magnifications; (**g**, **h**) X-ray photoelectron spectroscopy (XPS) analyses of C1s and F1s spectra, respectively. Stages I, II, and III represent the pristine state, after the 1st cycling, and after 400 cycles, respectively.

Structural and compositional evolution of the S@PAN electrodes

In our TzG@Si/S@PAN full cell system, manipulating the cycling voltage window, specifically the cut-off voltages of 1.0 V and 0.8 V, resulted in distinct differences in stability and capacity as shown in **Figure 3c-e**. This adjustment led to more pronounced changes in the real potential of the S@PAN cathode compared to the Si anode side (**Figure 3a**), underscoring the importance of studying the structural transformations and lithiation mechanisms of the S@PAN cathode. Such investigations could provide crucial insights into optimizing the S@PAN material for higher energy densities while ensuring its stability.

Operando Raman spectroscopy was employed as a vital tool to track the conversion of species and structural changes within the S@PAN matrix. The S@PAN-Li cell was discharged to 0.1 V prior to the measurements. As indicated in **Figure 5a** and **5b**, the observed peaks at 289 cm^{-1} and 366 cm^{-1} represent the bending of C–S bonds, while peaks at 480 cm^{-1} and 941 cm^{-1} are characteristic of S–S stretching, revealing the presence of sulfur chains (S_x) in the S@PAN composites. Additionally, two intense broad peaks at approximately 1326 cm^{-1} and 1552 cm^{-1} can be attributed to the D-band (disordered) and G-band (graphitic) respectively. The initiation of lithiation prompted the initial emergence of sulfur bond signals in the lower wavenumber range. Notably, no signals of lithium polysulfides Li_2S_x (where x = 6, 8) were detected throughout the cycling process, confirming the sulfur shuttle can be effectively mitigated by the S@PAN composite. [25]The peaks associated with the D and G bands demonstrated a shift and a decrease in the I_D/I_G ratio during discharge, which, however, partially restored but with diminished intensity after recharging. This behavior suggested that the carbonized structure of the S@PAN participated in lithium-ion storage, contributing to irreversible capacity during the first cycle.[26] Interestingly, at a discharge cut-off of 0.8 V, a peak at 800 cm^{-1} emerged and subsequently vanished, replaced by a new peak at 736 cm^{-1} not previously reported in the literature,

meriting further investigation. This peak at 800 cm^{-1} did not reappear in the second cycle, suggesting it may correspond to an intermediate species like ethylene carbonate-Li^+ (EC-Li^+) or fluoroethylene carbonate-Li^+ (FEC-Li^+).[27] The lowest feasible cut-off voltage was determined to be around 0.2 V, beyond which the electrode started undergoing a Li-Al alloying reaction.

Additionally, *ex situ* XPS was employed to comprehensively analyze the composition of the S@PAN electrodes at various stages of discharge: i) Pristine; ii) 1.0 V; iii) 0.8 V; iv) 0.2 V. Analyzing the S 2p spectra (**Figure 5c**) highlighted the primary reactive sites including C-S (162.3 eV, 163.5 eV), S-S_x (164.2 eV, 165.4 eV), which transitioned into C-S-Li and S_x-S-Li species. The S-N bonds also participated in the reactions, and deeper lithiation led to the cleavage of these Li-S-N and C-S-Li bonds, resulting in the formation of Li_2S. Notably, Li_2S was not detected above the cut-off voltage of 0.8 V. However, its presence was confirmed at the lower voltage of 0.2 V and was identified as amorphous through XRD analysis (**Figure S12**). In the C1s spectra (**Figure 5d**), peaks at 285.0 eV and 286.5 eV corresponding to C–C/C=C and C–S bonds in pristine S@PAN diminished after discharging. A significant peak at 290.0 eV indicative of C-F from PVDF was observed, overlapping with a strong peak of H-C-F and Li_2CO_3, which increased in intensity with deeper discharging due to the decomposition of carbonate electrolytes. Additionally, the F1s spectra indicated an increase in the ratios of both LiF (685.5 eV) and $Li_xPF_yO_z$ (688.5 eV) as discharging progressed, suggesting a higher rate of decomposition of the FEC component and $LiPF_6$ in the electrolyte. The capacity performance shown in **Figure S13** reveals that, even at a deeper cut-off voltage of 0.6 V, the S@PAN-Li cells maintained high capacity and exhibited robust capacity retention. This highlights the potential for further exploration of the capabilities of the S@PAN material through the manipulation of the voltage window.

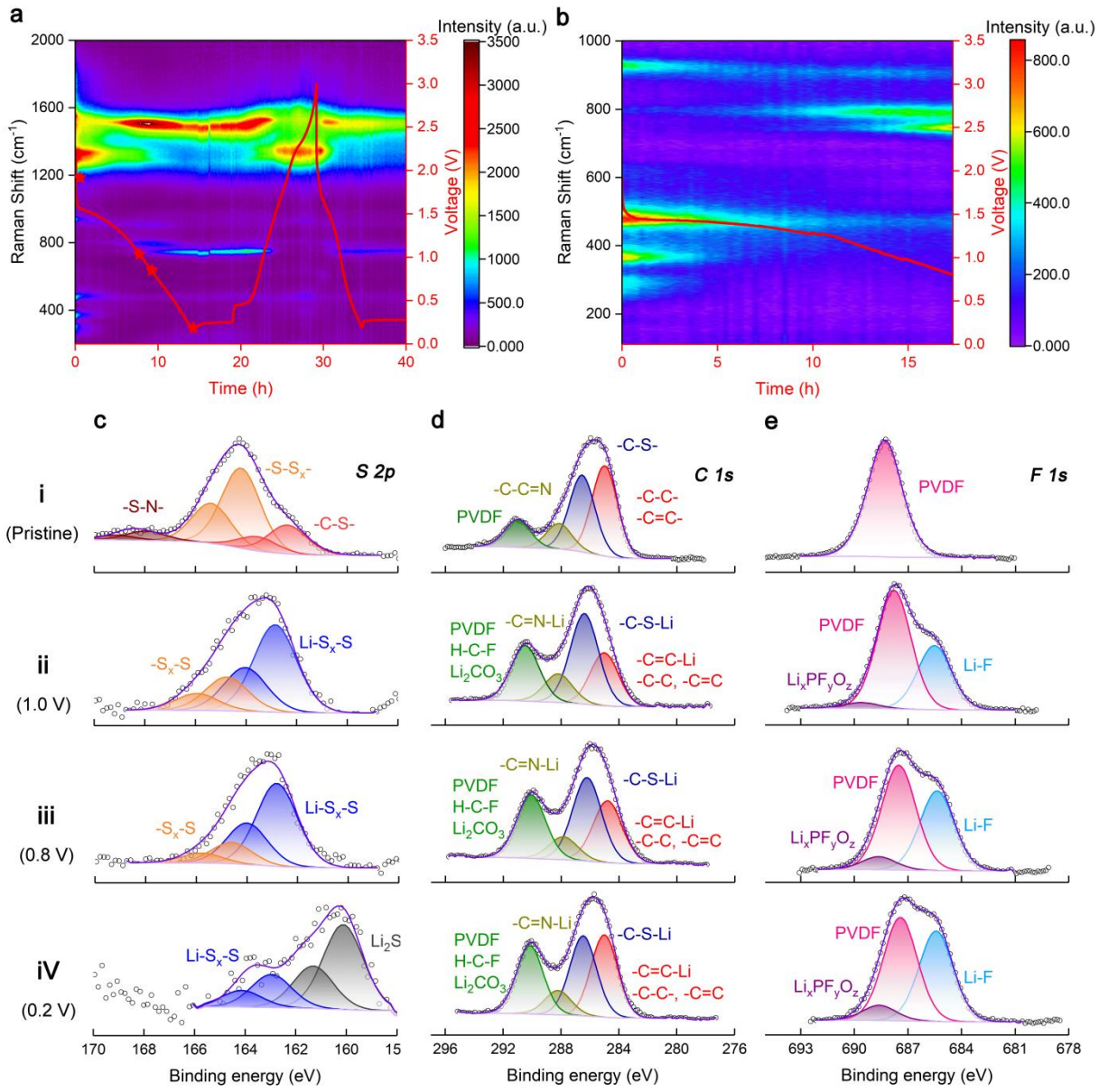

Figure 5. (**a**) Two-dimensional (2D) time-resolved Raman spectra of the S@PAN cathode. (**b**) Enlarged section of the Raman spectra from 200 cm^{-1} to 1000 cm^{-1}. (**c**, **d**, and **e**) X-ray photoelectron spectroscopy (XPS) analyses for S2p, C1s, and F1s, respectively. Stages **i**, **ii**, **iii**, and **iV** represent the different discharge stages of the disassembled S@PAN electrode, corresponding to the pristine state, 1.0 V, 0.8 V, and 0.2 V vs. Li^+/Li, respectively.

Conclusion

In summary, our development of a high-performance lithiated Si-S full cell system leverages the synergistic combination of a polymer-enhanced silicon (TzG@Si) anode and an organic polymer sulfur (S@PAN) cathode. Employing a compatible carbonate electrolyte, we established that both electrodes form a LiF-rich SEI layer, which crucially underpins the

stability of the entire cell. The robustness of the polymer backbone in each electrode ensures structural integrity throughout cycling, effectively mitigating the challenges of volume expansion. Additionally, *operando* Raman spectroscopy confirmed the absence of sulfur dissolution and migration. The full cell delivered an energy density of 414.3 Wh kg^{-1} and demonstrated enduring cycle life, sustaining performance over 400 cycles. These results underscore the substantial promise of this full cell system for future industrial applications.

Supporting Information

Acknowledgements

We thank Tobias Heinemann for SEM measurements, Kerstin Scheurell for ssNMR measurements. G.L. acknowledges the fellowship from the China Scholarship Council (CSC). This work was funded by the Federal Ministry of Education and Research (BMBF) T!Raum – TransferRäume für die Zukunft von Regionen“ GreenCHEM and the European Research Council (ERC) Proof of Concept Grant Scheme (LiAnMat-957534).

Received: ((will be filled in by the editorial staff))

Revised: ((will be filled in by the editorial staff))

Published online: ((will be filled in by the editorial staff))

References

[1] X. Shen, H. Liu, X.-B. Cheng, C. Yan and J.-Q. Huang, *Energy Storage Materials* **2018**, *12*, 161-175.
[2] T. Wang, T. Yang, D. Luo, M. Fowler, A. Yu and Z. Chen, *Small* **2023**, *n/a*, 2309306.
[3] Y. Yang, G. Zheng and Y. J. C. S. R. Cui, **2013**, *42*, 3018-3032.
[4] a) L. He, Q. Sun, L. Lu, S. J. A. A. M. Adams and Interfaces, **2021**, *13*, 34320-34331; b) X. Sun, M. Ouyang and H. J. J. Hao, **2022**, *6*, 1738-1742.
[5] C.-M. Park, J.-H. Kim, H. Kim and H.-J. Sohn, *Chemical Society Reviews* **2010**, *39*, 3115-3141.
[6] a) C. Chan, H. L. Peng and G. J. N. N. Liu, **2008**, *3*, 31-35; b) J. R. Szczech and S. Jin, *Energy & Environmental Science* **2011**, *4*, 56-72.
[7] a) A. Roland, J. Fullenwarth, J.-B. Ledeuil, H. Martinez, N. Louvain and L. Monconduit, **2022**, *1*, 20210009; b) Y. Lu, Z. Ye, Y. Zhao, Q. Li, M. He, C. Bai, X. Wang, Y. Han, X. Wan, S. Zhang, Y. Ma and Y. Chen, *Carbon* **2023**, *201*, 962-971.
[8] a) L. Deng, Y. Zheng, X. Zheng, T. Or, Q. Ma, L. Qian, Y. Deng, A. Yu, J. Li and Z. Chen, **2022**, *12*, 2200850; b) J. Song, M. Zhou, R. Yi, T. Xu, M. L. Gordin, D. Tang, Z. Yu, M. Regula and D. Wang, **2014**, *24*, 5904-5910; c) P.-F. Cao, G. Yang, B. Li, Y. Zhang, S. Zhao, S. Zhang, A. Erwin, Z. Zhang, A. P. Sokolov, J. Nanda and T. Saito, *ACS Energy Letters* **2019**, *4*, 1171-1180.
[9] a) Z. Cao, X. Zheng, Q. Qu, Y. Huang and H. Zheng, **2021**, *33*, 2103178; b) Y. Yang, Z. Yang, Z. Li, J. Wang, X. He and H. Zhao, **2023**, *13*, 2302068.
[10] J. Wang, J. Yang, J. Xie and N. Xu, **2002**, *14*, 963-965.
[11] J. Huang, A. Martin, A. Urbanski, R. Kulkarni, P. Amsalem, M. Exner, G. Li, J. Müller, D. Burmeister, N. Koch, T. Brezesinski, N. Pinna, P. Uhlmann and M. J. Bojdys, **2022**, *2*, e20210105.
[12] R. Kulkarni, J. Huang, M. Trunk, D. Burmeister, P. Amsalem, J. Müller, A. Martin, N. Koch, D. Kass and M. J. Bojdys, *Chemical Science* **2021**, *12*, 12661-12666.
[13] D. Schwarz, Y. Noda, J. Klouda, K. Schwarzová-Pecková, J. Tarábek, J. Rybáček, J. Janoušek, F. Simon, M. V. Opanasenko and J. J. A. M. Čejka, **2017**, *29*, 1703399.
[14] S. Wei, L. Ma, K. E. Hendrickson, Z. Tu and L. A. Archer, *Journal of the American Chemical Society* **2015**, *137*, 12143-12152.
[15] M. A. Weret, C.-F. Jeffrey Kuo, T. S. Zeleke, T. T. Beyene, M.-C. Tsai, C.-J. Huang, G. B. Berhe, W.-N. Su and B.-J. Hwang, *Energy Storage Materials* **2020**, *26*, 483-493.
[16] C.-J. Huang, K.-Y. Lin, Y.-C. Hsieh, W.-N. Su, C.-H. Wang, G. Brunklaus, M. Winter, J.-C. Jiang and B. J. Hwang, *ACS Applied Materials & Interfaces* **2021**, *13*, 14230-14238.
[17] S. Hansen, E. Quiroga-González, J. Carstensen and H. Föll, *Electrochimica Acta* **2016**, *217*, 283-291.
[18] Y. Li, S. Zhang, H. Liu, Y. Zhang and X. Zhang, *ACS Applied Energy Materials* **2023**, *6*, 8511-8520.
[19] P. Xu, X. Hu, X. Liu, X. Lin, X. Fan, X. Cui, C. Sun, Q. Wu, X. Lian, R. Yuan, M. Zheng and Q. Dong, *Energy Storage Materials* **2021**, *38*, 190-199.
[20] R. Shang, T. Zerrin, B. Dong, C. S. Ozkan, M. J. T. Ozkan and Innovation, **2020**, *21*, 1-23.
[21] H. Yang, C. Guo, J. Chen, A. Naveed, J. Yang, Y. Nuli and J. Wang, **2019**, *58*, 791-795.
[22] J. Sung, N. Kim, J. Ma, J. H. Lee, S. H. Joo, T. Lee, S. Chae, M. Yoon, Y. Lee, J. Hwang, S. K. Kwak and J. Cho, *Nature Energy* **2021**, *6*, 1164-1175.

[23] C. Xu, F. Lindgren, B. Philippe, M. Gorgoi, F. Björefors, K. Edström and T. Gustafsson, *Chemistry of Materials* **2015**, *27*, 2591-2599.
[24] Z.-Q. Jin, Y.-G. Liu, W.-K. Wang, A.-B. Wang, B.-W. Hu, M. Shen, T. Gao, P.-C. Zhao and Y.-S. Yang, *Energy Storage Materials* **2018**, *14*, 272-278.
[25] a) S. Zhang, **2013**, *1*; b) X. Wu, Y. Zhao, H. Li, C. Zhou, X. Wang and L. Du, *Nanoscale* **2024**, *16*, 5060-5078.
[26] X. Wang, Y. Qian, L. Wang, H. Yang, H. Li, Y. Zhao and T. Liu, **2019**, *29*, 1902929.
[27] K. Hiraoka and S. Seki, *The Journal of Physical Chemistry C* **2023**, *127*, 11864-11874.